

Gene Transfer Corrects Acute GM2 Gangliosidosis—Potential Therapeutic Contribution of Perivascular Enzyme Flow

M Begoña Cachón-González¹, Susan Z Wang¹, Rosamund McNair¹, Josephine Bradley¹, David Lunn², Robin Ziegler³, Seng H Cheng³ and Timothy M Cox¹

¹Department of Medicine, University of Cambridge, Cambridge, UK; ²Medical Research Council Biostatistics Unit, Institute of Public Health, Cambridge, UK; ³Genzyme Corporation, Framingham, Massachusetts, USA

The GM2 gangliosidoses are fatal lysosomal storage diseases principally affecting the brain. Absence of β -hexosaminidase A and B activities in the Sandhoff mouse causes neurological dysfunction and recapitulates the acute Tay–Sachs (TSD) and Sandhoff diseases (SD) in infants. Intracranial coinjection of recombinant adeno-associated viral vectors (rAAV), serotype 2/1, expressing human β -hexosaminidase α (HEXA) and β (HEXB) subunits into 1-month-old Sandhoff mice gave unprecedented survival to 2 years and prevented disease throughout the brain and spinal cord. Classical manifestations of disease, including spasticity—as opposed to tremor-ataxia—were resolved by localized gene transfer to the striatum or cerebellum, respectively. Abundant biosynthesis of β -hexosaminidase isozymes and their global distribution via axonal, perivascular, and cerebrospinal fluid (CSF) spaces, as well as diffusion, account for the sustained phenotypic rescue—long-term protein expression by transduced brain parenchyma, choroid plexus epithelium, and dorsal root ganglia neurons supplies the corrective enzyme. Prolonged survival permitted expression of cryptic disease in organs not accessed by intracranial vector delivery. We contend that infusion of rAAV into CSF space and intraparenchymal administration by convection-enhanced delivery at a few strategic sites will optimally treat neurodegeneration in many diseases affecting the nervous system.

Received 16 September 2011; accepted 12 February 2012; advance online publication 27 March 2012. doi:10.1038/mt.2012.44

INTRODUCTION

The GM2 gangliosidoses are fatal inherited neurodegenerative diseases, principally affecting infants and young children, for which there is no effective treatment. Rare attenuated adult forms also occur.¹

Mutations in the genes encoding β -hexosaminidase α (HEXA) and β (HEXB) subunits, and GM2-activator protein (GM2A), cause Tay–Sachs disease (TSD), Sandhoff–Jatzkewitz disease, and GM2 activator deficiency, but clinically these conditions

are indistinguishable.^{2–5} Hex A isozyme requires dimerization of α and β subunits for enzymatic activity, whereas Hex S and Hex B are homodimers of α and β subunits, respectively.^{6–8} Of the stored glycoconjugates only ganglioside GM2 has an absolute requirement for Hex A and cofactor GM2-activator protein for its breakdown.⁹ Failure to cleave β -N-acetyl-hexosamine residues from the nonreducing ends of glycoconjugates leads to lysosomal storage in neural tissue and relentless neurodegeneration. In common with many other neurological insults, there is activation of microglia/macrophages and astrocytes with concomitant production of inflammatory mediators.¹⁰ The inflammatory response may precede the clinical manifestations,¹¹ and further perpetuate neurological injury.¹²

GM2 gangliosidoses occur naturally in several species,^{13,14} but the mouse is more amenable for testing new therapies. Two Sandhoff mouse models have been generated by targeted disruption of the *Hexb* gene.^{15,16} Sandhoff mice appear normal for about the first three months of life, but thereafter they rapidly deteriorate and die between the age of 4 and 5 months. Glycoconjugate accumulation extends to most regions of the brain and spinal cord. Motor dysfunction, which includes spasticity, muscle weakness, rigidity, tremor and ataxia is stereotypic and reflects disease in the cerebrum and cerebellum. The manifestations of disease in Sandhoff mice closely mirror those observed in the acute form of GM2 gangliosidosis in human infants.

GM2 gangliosidosis mouse models have been extensively used in the search for an effective treatment of these devastating diseases. Approaches taken include substrate reduction therapy,¹⁷ bone marrow,¹⁸ and neural stem cell transplantation,^{19,20} anti-inflammatory drugs,²¹ intraventricular delivery of purified protein,²² and adenoviral²³ and lentiviral vectors²⁴ driving expression of the corrective enzyme. Unfortunately, survival and functional outcomes of these therapies have been modest. Pharmacological chaperons²⁵ are being tested in clinical trials, but these are predicted to benefit late-onset forms where residual enzyme is present.

We have previously shown that intracranial delivery of recombinant adeno-associated viral vectors (rAAV) expressing the β -subunit of β -hexosaminidase (rAAV β) alone delays disease onset in the Sandhoff mouse. It has been predicted however, that in both TSD and SD, overexpression of one of the transgenes would

Correspondence: M Begoña Cachón-González, Department of Medicine, University of Cambridge, Level 5, Box 157, Addenbrooke's Hospital, Hills Road, Cambridge CB2 0QQ, UK. E-mail: mcb23@medschl.cam.ac.uk

rapidly deplete the pool of its endogenous subunit partner. Since successful clinical application of gene therapy will require robust synthesis of Hex A, simultaneous coexpression of α and β subunits is necessary.^{23,26} Coinjection of low-titer rAAV-expressing human β -hexosaminidase α (rAAV α) and β subunits (rAAV α + rAAV β), allowed survival of 20% of the animals to at least 1 year of age.²⁷

To inform the design of therapeutic trials in human patients, we set out to define: (i) the minimum number of injections necessary to achieve global delivery of enzyme to the brain and spinal cord for complete resolution of disease; (ii) those sites in the brain with connections that would promote axonal transport of the viral vectors and distribution of β -hexosaminidase; and (iii) whether it is possible to use therapeutic gene transfer to discriminate between the different contributions of disease in the cerebral cortex and cerebellum to spasticity or tremor and ataxia, respectively. Here, we report: 100% survival to >1 year and minimal residual pathological changes in the brain and spinal cord is achieved with few injections at high vector dose; that salutary outcomes correlate with prominent movement of corrective enzyme within perivascular and cerebrospinal fluid (CSF) spaces, within and along axonal tracts and diffusing from injection sites; classical signs of disease, namely spasticity and tremor/ataxia, can be corrected independently—finally, that in the absence of targeted delivery, emerging disease with pathological storage develops at peripheral sites in long-term survivors.

RESULTS

Abundant activities of all three Hex isozymes are generated by intracranial coinjection of 2/1 rAAV α + rAAV β

We infused 1-month-old mutant Sandhoff mice (SD) with rAAV β or rAAV α + rAAV β at a single site into the striatum and sacrificed them 4 weeks postinjection. Wild type and TSD animals were used as controls. Cerebrum or liver from controls, and transduced hemispheres were homogenized and tissue extracts subjected to ion-exchange chromatography or cellulose-acetate electrophoresis to separate Hex isozymes; the fluorogenic substrate 4-MUG was used to detect the activity of all three isozymes while 4-MUGS was used to indicate the presence of Hex A and S. We show that brain transduced with rAAV α +rAAV β expresses abundant Hex A, Hex B, and Hex S isozymes. When rAAV β alone was infused, expression of only the Hex B isozyme was detected (Figure 1a–d,f). The expected pattern of mature α (α_m) and β (β_m ”a,” β_m ”b,” and β_m ”c”) subunits was verified by polyacrylamide gel electrophoresis and western blotting with an antibody against Hex A on brain extracts and relevant fractions from chromatographic separation (Figure 1e). We ascribe the interspecies isozyme mobility differences to variations in amino acid composition and the positively charged HIV1-tat domain fused to recombinant human β -hexosaminidase polypeptides. Dual *in situ* hybridization (ISH) fluorescence microscopy of rAAV α + rAAV β -transduced brain sections with subunit-specific RNA probes showed that most transduced cells expressed both subunits, albeit at varying ratios (Figure 1g).

Survival is enhanced in a rAAV α + rAAV β dose and site-dependent manner

We compared therapeutic outcomes of infusions of rAAV α + rAAV β in 1-month-old SD mice according to distinct experimental

protocols: unilaterally into the striatum (Sx1), bilaterally into the striatum (Sx2) or cerebellum (Cx2), and bilaterally into the striatum and cerebellum (S+C) or into the hippocampus and cerebellum (H+C). Mannitol was added as a coinjectant to aid rAAV diffusion. The same 2/1 rAAV α and rAAV β vector batches were used throughout the study to reduce variability. Maintenance of body weight and coat condition was monitored regularly as indicators of well-being and fitness.

Survival was analyzed with the log-rank (Mantel–Cox) test: intracranial rAAV-mediated gene delivery has a marked effect on the life-span of this acute mouse model of GM2 gangliosidosis ($P < 0.0001$), as shown by the Kaplan–Meier plot (Figure 2a). Survival of the different treatment groups was examined by one-way analysis of variance and adjusted for multiple *post-hoc* comparisons by the Bonferroni method. Median survival was 730 days for untreated normal controls (wild type and heterozygous) ($n = 22$) and 131 days for mutant animals [SD (UT)] ($n = 37$). In contrast, median survival of groups of SD mice treated according to the different protocols was in the order: S+C (681 days, $n = 16$); H+C (609 days, $n = 8$); Cx2 (595 days, $n = 8$); Sx2 (455 days, $n = 8$); Sx1 (194 days; $n = 15$). The vector delivery protocols with the best survival outcome were S+C and H+C with no significant difference between these cohorts ($P > 0.05$) suggesting that the accrued benefit was similar. The S+C combination was superior to either Sx2 or Cx2 alone ($P < 0.05$). Although no clear difference in apparent survival between H+C and Sx2 or Cx2 was returned ($P > 0.05$), the neurological effects of the interventions differed markedly between the groups. See **Supplementary Table S1** for details on the cause of death in all animals in the study.

Long-term survival of mice injected bilaterally into a single structure, Sx2 and Cx2, was unexpected. Distribution of survival within the Cx2 group was particularly striking: the animals either overlapped with those singly injected or those with best outcomes in groups S+C and H+C as depicted in the scatter plot (Figure 2b). Between groups Cx2 and Sx2 survival was not significantly different, but the manifestations of disease differed considerably. We attribute much of the variation in the outcome of single injections to technical difficulties inherent to the delivery of microlitre quantities manually into a small brain. However, even the best outcomes from single-site interventions were insufficient to secure long-term rescue of disease with its global effects in the nervous system.

Growth of mutant mice declines sharply during the last month of life, but successful rAAV α +rAAV β treatment prevents this decline (Figure 2c and **Supplementary Figure S1**).

Treated SD mice have reduced adipose tissue and are generally smaller than their normal littermates but grooming is well maintained and their coat appears healthy.

Biodistribution of vector and enzyme depends only partly on therapeutic modality

Transduced cells were identified by ISH with antisense and sense RNA probes against the common WPRE-BGHpA sequence. Tissue structures labeled by ISH are documented in **Supplementary Table S2**; these are named using the nomenclature of Franklin and Paxinos.²⁸ Histochemical staining for β -hexosaminidase activity

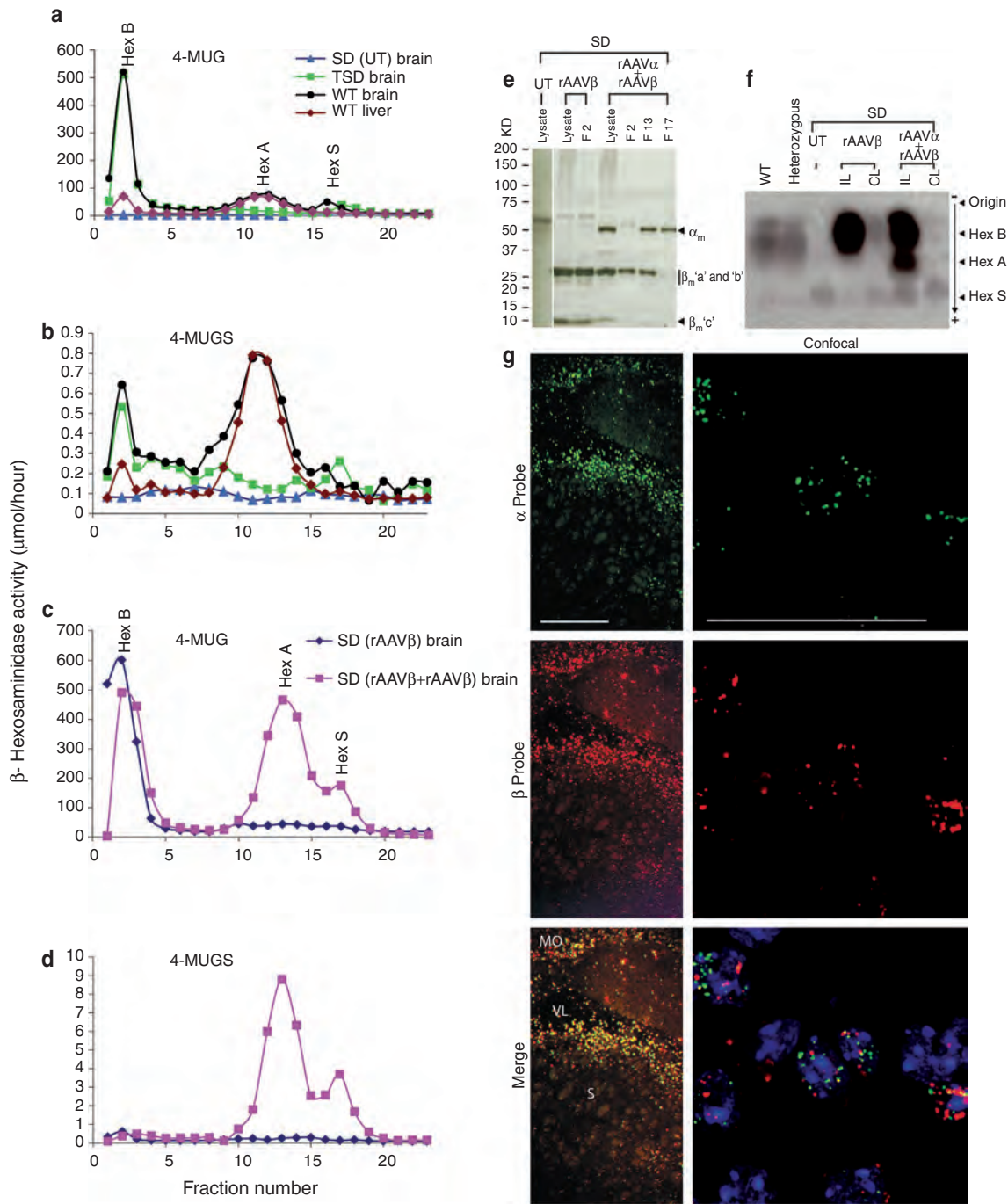


Figure 1 β-Hexosaminidase profile of mouse tissues. **(a–d)** Representative activities of β-hexosaminidase isozymes Hex A, Hex B, and Hex S in liver or brain extracts separated by ion-exchange chromatography; wild type (WT), untreated (UT), Sandhoff (SD), and Tay–Sachs (TSD) disease mice; rAAVβ or rAAVα+rAAVβ transduced brain was analyzed 4 weeks postinjection. Activities of 5 μl samples were determined against substrates 4-MUG and 4-MUGS, and normalized to 100 μg of loaded protein. **(e)** β-Hexosaminidase polypeptide components resolved by sodium dodecyl sulfate-polyacrylamide gel electrophoresis (SDS-PAGE), and immunoblotted with goat antihuman Hex A: unfractionated lysate (lysate) and fractions 2 (F 2), 13 (F 13) and 17 (F 17) in panels **c** and **d**. α_m, mature α subunit; β_m“a,” β_m“b,” and β_m“c,” proteolysed species of mature β subunit. Standards are given in kDa. **(f)** Cellulose-acetate electrophoresis of extracts from WT, *hexB* heterozygous, and SD mouse cerebrum injected at a single striatal site. Isozymes from ipsilateral (IL) and contralateral (CL) hemispheres revealed by incubation with 4-MUG. Micrograms of total protein loaded (from left to right): 103, 108, 242, 120, 128, 185, and 229. **(g)** Human α and β subunits RNA detected in SD (rAAVα+rAAVβ) brain sections by *in situ* hybridization with fluorescein and cyanine-3-conjugated tyramide signal amplification reagent, respectively. Mice were injected at one month and killed aged 2 years. Diamidino-2-phenylindole (DAPI)-stains cell nuclei blue. Bars: 200 μm (left panels in **g**); 50 μm (right panels in **g**). rAAV, recombinant adeno-associated viral vectors.

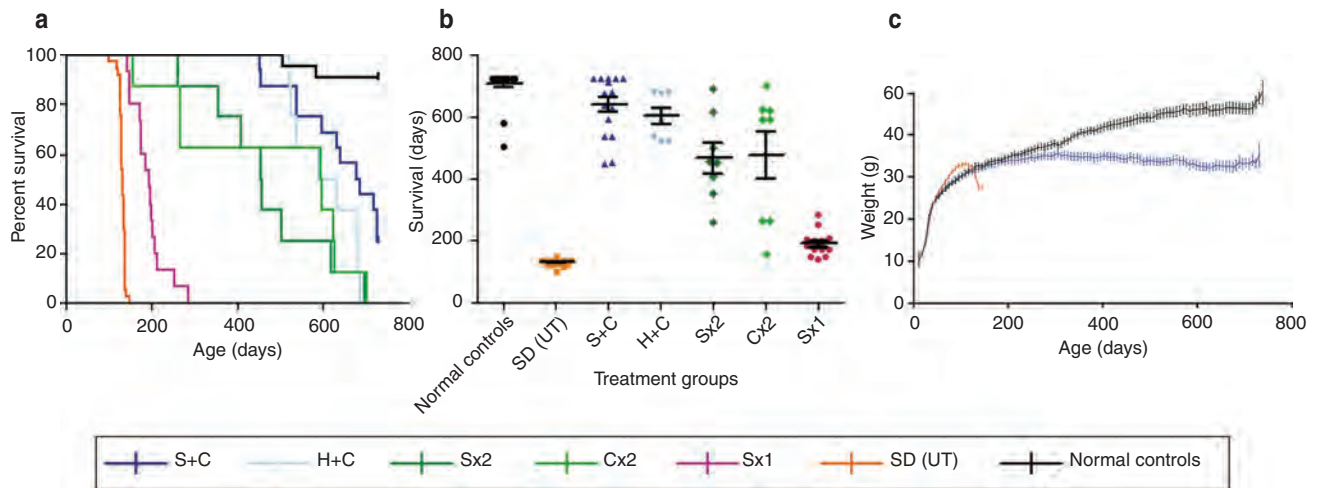


Figure 2 Lifespan of Sandhoff mice after intracranial infusions of rAAV α +rAAV β at 1 month of age. **(a)** Kaplan–Meier survival curve, data censored at 2 years. Sandhoff (SD) mice were injected unilaterally into the striatum (Sx1, $n = 15$), bilaterally into the striatum (Sx2, $n = 8$) or cerebellum (Cx2, $n = 8$), and bilaterally into the striatum and cerebellum (S+C, $n = 16$) or into the hippocampus and cerebellum (H+C, $n = 8$). Control groups: untreated normal controls ($n = 22$) and SD mice [SD (UT), $n = 37$]. **(b)** One-way analysis of variance (ANOVA) and Bonferroni multiple *post-hoc* comparisons with mean \pm SEM. **(c)** Comparison of average weekly weights for S+C-treated, normal controls and SD (UT) groups. The mean \pm 1.96 SE are plotted against the mid-point of each week. rAAV, recombinant adeno-associated viral vectors.

was carried out in consecutive sections. A systematic analysis was performed on sections from five S+C, one H+C, one Sx2, and two Cx2-injected animals.

Injections into the striatum induced widespread distribution of virus and enzyme. Staining was most intense at the injection site and interconnected areas. Dissemination was further amplified by the ability of the virus to disperse along white matter such as corpus callosum (Figure 3a).

ISH and β -hexosaminidase activity labeled choroid plexus (Figure 3a,b)—by leakage and/or diffusion of infusate into the ventricular/subarachnoid space, cells around penetrating ventral spinal roots (Figure 3c), and dorsal root ganglia (Figure 3d). Histochemical staining for hexosaminidase was prominent in sciatic nerves (Figure 3e), consistent with spread of vector to distant dorsal root ganglia in the CSF, and dorsal roots and dorsal columns of the spinal cord (Figure 3f). Furthermore, ISH and hexosaminidase staining was detected extracranially in periocular (Figure 3g) and subcutaneous muscle of the eyelid (Figure 3h), and the perineurium of cranial nerves such as the optic nerves (Figure 3g). We attribute this to vector distribution via the CSF.

Viral infusions into the hippocampus led to ISH-labeling of the hippocampal formation and interconnected regions.

Injections into the deep cerebellar nuclei led to delivery of vector and enzyme to most layers of the cerebellar cortex and interconnected areas (Figure 4a,b), but we also found diffusion or leakage of vector into adjacent cerebellar and brain stem white matter, such as middle cerebellar peduncle (Figure 4a). Cells staining by ISH in white matter closely resembled oligodendrocytes, but may also represent other glia (Figure 4b). Diffusion of virus extended into brain stem nuclei, with some variability encountered between animals and between injected hemispheres of the same animal (Figure 4a).

Diffusion into structures adjacent to the deep cerebellar nuclei, particularly into the highly interconnected brain stem nuclei, might explain spread to unexpected brain regions. This proposition is best exemplified by results from Cx2-injected animals with contrasting functional outcomes. The brain of an animal with severe neurological disease (Supplementary Video S6), had ISH and Hex-specific staining which was highly restricted to the cerebellum; moreover abundant storage material was present in both sides of the brain, such as in the forebrain. In marked contradistinction, a mouse with few signs of disease (Supplementary Video S7), and strong ISH-labeling in the right cerebellum and brain stem had its entire right brain almost free of storage. In this animal, ISH staining was weak in the left cerebellum and almost absent in the left brain stem; more pathological storage was observed in the left side of the brain (Figure 4a and c, and Supplementary Figure S2). Only a faint histochemical reaction for β -hexosaminidase activity was detectable under the microscope in either cerebral hemisphere of this mouse. Small differences in hexosaminidase activity, reflecting the asymmetric gene transduction of hindbrain, seem likely to account for the marked differences in the expression of disease in the brain observed within the same animal. In these studies, every attempt was made to infuse equal volumes of vector preparation bilaterally into the brain, but experience has long shown that the side first injected generally gives the strongest signal for vector genome by ISH and histochemical staining for β -hexosaminidase.

One of the most striking findings was that much of the distribution of β -hexosaminidase activity stain occurred in a pattern resembling that of cerebral blood vessels of various diameters, particularly notable in long-lived animals. High magnification revealed capillary structures staining for enzyme in brain regions remote from the site of vector injection—even as far as the spinal cord (Figure 5a). The enzymatic stain was in close proximity to structures labeled with fluoresceinated

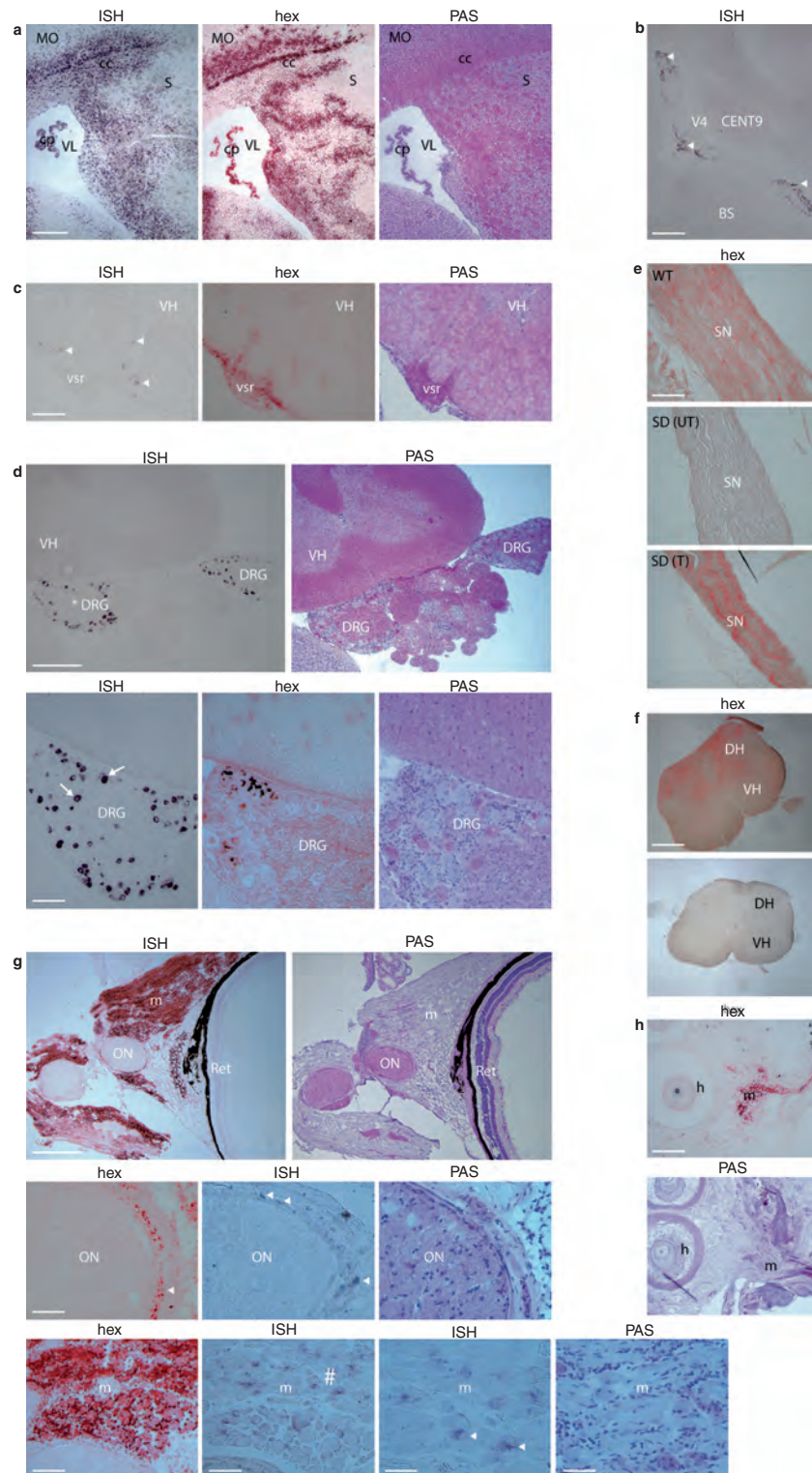


Figure 3 Biodistribution of viral vector and enzyme. **(a-d)** Detection of vector RNA on sections from Sandhoff (SD) mice injected with rAAV α +rAAV β into the striatum at one month of age by *in situ* hybridization (ISH, black stain). ISH stained: gray and white matter, such as **(a)** corpus callosum (cc); choroid plexus (cp) in all ventricles, including that in **(a)** lateral ventricles (VL), and **(b)** 4th ventricle (V4) (arrowheads); ventral roots of the **(c)** spinal cord (vsr) (arrowheads); and **(d)** dorsal root ganglia (DRG) (arrows in magnified view of asterisk region). Consecutive sections stained for enzyme (hex), red precipitate, positively correlated with ISH-labeled regions, as shown in panels **a**, **c**, and **d**. Enzyme was present in **(e)** sciatic nerve; and **(f)** spinal cord and roots (top panel treated, bottom panel untreated SD). Vector RNA and enzyme was found extracranially in the orbit, around optic nerve (ON) (arrowheads) and periocular muscle (m) (arrows in magnification of area with hash symbol) **(g)**; and **(h)** subcutaneous muscle supporting hair follicles. Consecutive sections stained with periodic acid-Schiff (PAS) for structure identification. Wild type (WT), untreated [SD (UT)] and rAAV α +rAAV β -treated [SD (T)] Sandhoff mice. Brain stem (BS); dorsal horn (DH); motor cortex (MO); ninth cerebellar lobule (CENT9); retina (Ret); striatum (S); ventral horn (VH). Bars: 500 μ m (**a**, **f**, top panels in **d** and **g**); 200 μ m (**e**, **h**, and lower panels in **d**); 100 μ m (**b**, **c**; and first and second left lower panels in **g**); 50 μ m (middle panels in **g**; and third and fourth right lower panels in **g**). rAAV, recombinant adeno-associated viral vectors.

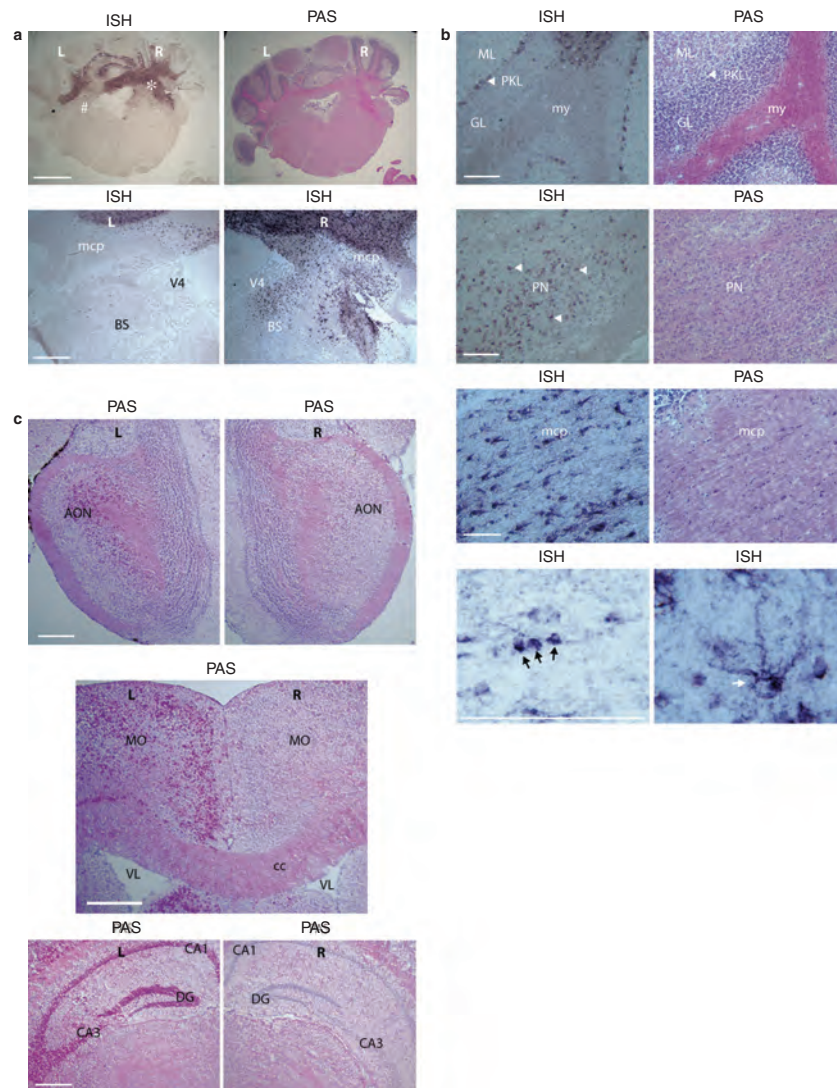


Figure 4 Resolution of pathology in brain regions distant from injected sites. **(a)** *In situ* hybridization (ISH) staining, black precipitate, for vector RNA of sections from a Cx2-injected SD mouse was heaviest in right cerebellum and dorsal brain stem nuclei (BS) (top left panel and magnified views of hash and asterisk areas in lower panels). **(b)** ISH stained Purkinje cell layer (PKL), and pontine nucleus (PN) (arrowheads). Cells in white matter, such as middle cerebellar peduncle (mcp), had oligodendrocytic (black arrows) or other glial (white arrow) morphologies. **(c)** In this animal, injected at 1 month and killed at 628 days of age (**Supplementary Video S7**, viewed at 1 year), glycoconjugate accumulation, magenta stained with periodic acid-Schiff (PAS) reagent, was principally found in left brain; shown are olfactory bulbs (top panels), motor cortex (MO) (middle panels), and hippocampus (lower panels). Anterior olfactory nucleus, medial part (AOM); field CA1 and CA3 of hippocampus; corpus callosum (cc); dentate gyrus (DG); fourth ventricle (V4); lateral ventricle (VL); molecular (ML) and granular (GL) layers of the cerebellar cortex; myelin tracts (my); right (R) and left (L) hemispheres. Bars: 2 mm (top panels in **a**); 500 μ m (**c** and lower panels in **a**); 200 μ m (from top: first and second set of panels in **b**); 100 μ m (from top: third and fourth set of panels in **b**).

tomato lectin, which selectively binds to endothelium. In brain regions where β -hexosaminidase appeared to be predominantly “perivascular,” *e.g.*, in the forebrain (**Figure 5a–c**) and the brain stem (**Figure 5a**), little storage or neuroinflammation could be found (**Supplementary Figure S3**).

S+C or H+C viral infusions prevent the manifestations of GM2 gangliosidosis

We chose the S+C route because these structures have intricate connections with large regions of the brain early affected in GM2 gangliosidosis. The hippocampus, a critical centre for memory, is a discrete, self-contained unit and thus would limit

virus and enzyme distribution. We reasoned that by comparing the therapeutic outcomes of these two interventions, the principal biodistribution pathways would be readily distinguished from alternative routes of dissemination.

The brains and spinal cords of six long-surviving SD mice from groups S+C (five animals) and H+C (one animal) were examined histologically and stained with GM2 antibody or the periodic acid-Schiff (PAS) reagent to detect GM2 ganglioside and other stored glycoconjugates. Unexpectedly, there was a striking absence of neuronal storage in the brains and at all levels of the spinal cord in these aged mice (**Supplementary Figure S4** and **Figure 5d**). Moreover, neuroinflammation, as assessed

by the intensity and number of cells staining for the microglia/macrophage (CD68) and astrocytic (GFAP) markers, was greatly reduced in treated animals compared with untreated SD mice (**Supplementary Figure S3**). Irrespective of the intervention used to transfer the therapeutic genes, and where at all observed, the inflammatory response was local and commensurate with the levels of pathological storage (**Figure 6a**). Absence of neuropathological changes directly correlated with preservation of neurological function in long-surviving Sandhoff mice (**Supplementary Videos S1–S3**).

Tremor and ataxic gait can be segregated from spastic disease

To determine the extent of disease rescue for a given brain region and whether it is possible to use gene transfer to discriminate between the different neurological manifestations of GM2 gangliosidosis anatomically, SD mice were injected with vector bilaterally at two distant, and poorly interconnected sites in the brain. These sites were the deep cerebellar nuclei (Cx2) or the striatum (Sx2). Positioned 6-mm apart, both regions are well connected to other parts of the brain and were expected to distribute the corrective enzyme widely—but with little overlap. The deep cerebellar nuclei carry the main output of the cerebellum and receive important inputs from Purkinje layer; the striatum has afferent connections and efferent output to key motor control areas such as motor cortex, thalamus, brainstem and other parts of basal ganglia.

Throughout their lives, 30% of the Sx2-injected animals had no overt neurological signs and the remainder had mild tremor and ataxia which was delayed in onset, and remained stable—manifestations which indicate disease of the cerebellum or its connections (**Supplementary Videos S4 and S5**). Brain and spinal cord coronal sections from a representative SD animal aged 619 days with mild disease were stained with the PAS reagent at every 180 μ m. These studies showed that most neurons in the brain and spinal cord were free of pathological storage, except for PAS-positive cells in cerebellar cortex. Compared with the cerebellum of untreated animals at their humane end point the abundance of storage material was greatly diminished (**Figure 6a**). In the spinal cord PAS-positive neurons were rare.

Two-thirds of Cx2-injected mice either had no overt disease or had a disease that consisted mainly of claspings of hind limbs when lifted by the tail; they walked with the body close to the ground. These signs remained unchanged throughout, and occurred in the absence of tremor or ataxia. Mean survival for this subgroup was 629 days. The remaining one third developed a severe and progressive wasting disease characterized by dragging of hind limbs with elevated pelvis, but without tremor or ataxia (**Supplementary Video S6**). Animals in this adverse subgroup lost weight rapidly and required humane killing; mean survival was 229 days. The neurological signs in the Cx2-injected group indicate spasticity due to disease of cerebral cortical neurons or their connections. GM2 antibody staining

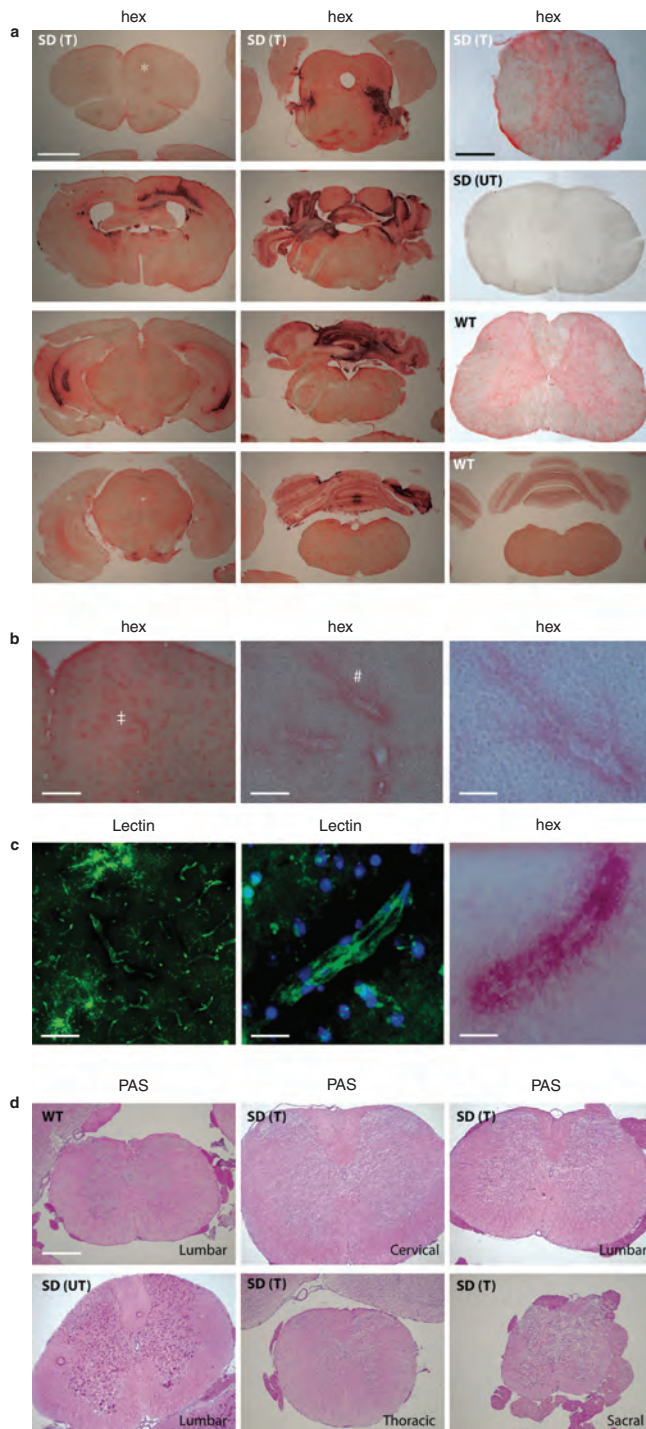


Figure 5 β -Hexosaminidase with prominent perivascular localization reduces glycoconjugate storage throughout the neuraxis. **(a)** In a representative S+C-injected Sandhoff mouse [SD (T)] β -hexosaminidase stain (hex), red precipitate, was found throughout the brain (shown from top left to middle lower panel: forebrain through to hindbrain), and spinal cord (top rightmost panel); viewed at 1 and 2 years of age in **Supplementary Videos S2 and S3**. Controls: 4-month untreated Sandhoff [SD (UT)] (**Supplementary Video S1**) and 2-year-old wild type (WT). **(b)** Much of the enzyme stain appears perivascular; magnified views: area of asterisk in **a** (left panel), cross (middle panel) and hash (right panel) areas in **b**. **(c)** Costaining of hex with fluorescein-conjugated tomato lectin to label endothelium, showed close association—with hex also distributed away from the fluorescein label seen as a dark halo (left and middle panels). Diamidino-2-phenylindole (DAPI) stains cell nuclei blue. **(d)** Glycoconjugate material (magenta), stained with periodic acid-Schiff (PAS) reagent, at different levels of the spinal cord. Bars: 2 mm (brain panels in **a**); 500 μ m (spinal cord panels in **a** and **d**; and left panel in **b**); 200 μ m (left panel in **c**); 100 μ m (middle panel in **b**); 50 μ m (right panel in **b**, middle and right panels in **c**).

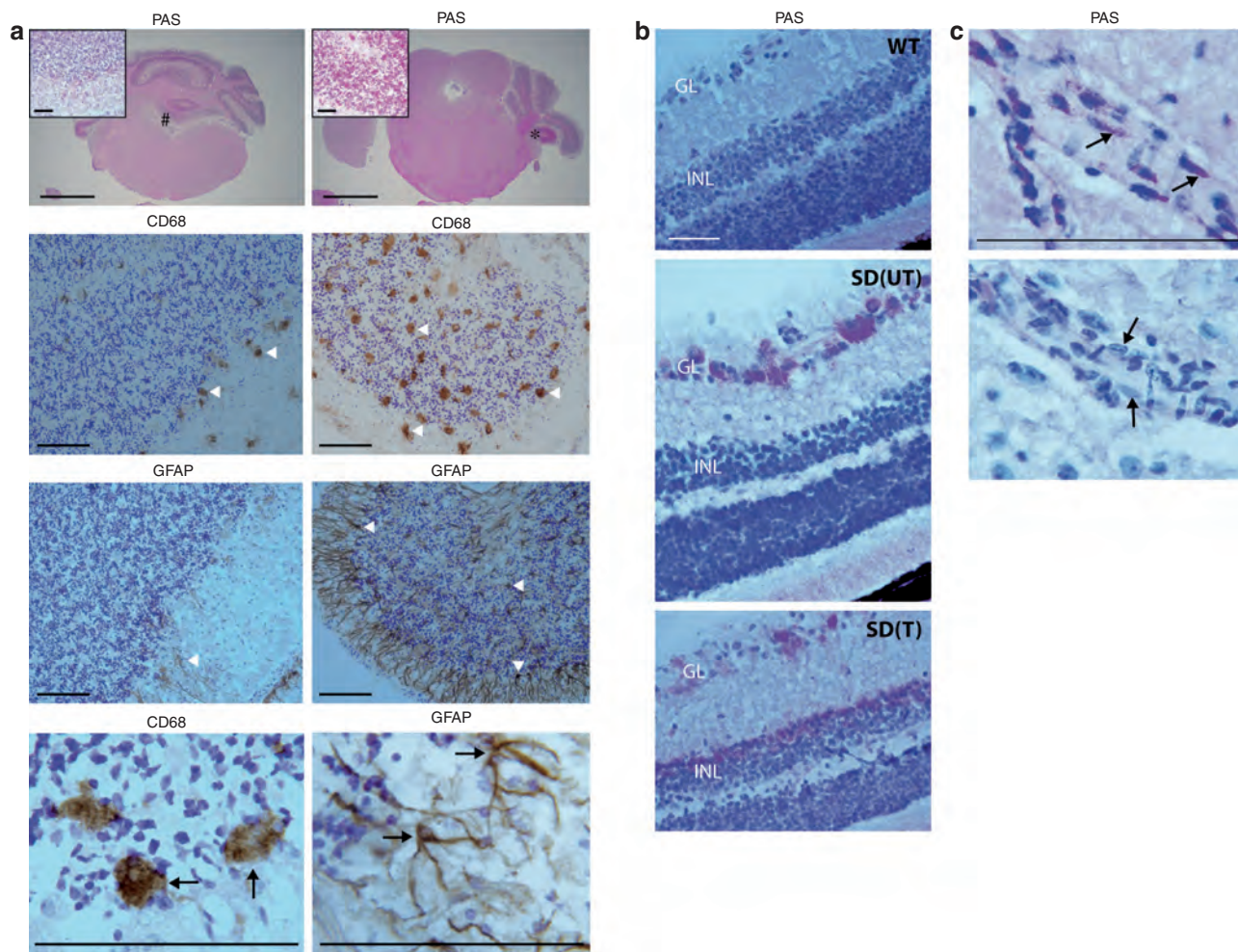


Figure 6 Inflammatory response in the presence of residual storage and emerging disease in nontargeted tissues. **(a)** The intensity and number of cells staining for the microglial marker, CD68, and astrocytic marker, GFAP, correlated with local glycoconjugate abundance (stained magenta with periodic acid-Schiff (PAS) reagent). Displayed are sections from an Sx2-injected Sandhoff (SD) mouse, killed at 696 days and viewed in **Supplementary Videos S4** and **S5** at 12 and 20 months of age. The ninth cerebellar lobule with few PAS-stained neurons (hash area and inset in left panel) had few cells labeled with CD68 (arrowheads in left panel) and GFAP (arrowhead in left panel). In contrast, the flocculus lobe with many intensely PAS-stained neurons (asterisk area and inset in right panel) had many cells labeled with CD68 (arrowheads, right panel) and GFAP (arrowheads, right panel). Globular microglia (arrows in left bottom panel) and astrocytes (arrows, right bottom panel) are intensely stained. **(b)** Abundant periodic acid-Schiff (PAS)-stained glycoconjugate was found in retinal ganglion cell layer (GL) in 4-month untreated SD [SD (UT)] compared with 2-year-old wild type (WT). In S+C-treated 2 year-old SD [SD (T)] staining was found in GL and inner nuclear (INL) layers. **(c)** SD (T) mouse endothelium in regions with low activity of β -hexosaminidase contained PAS-stained glycoconjugates (arrows, top panel), but staining was undetectable in regions with abundant enzyme activity such as those close to injection sites (arrows in lower panel). Bars: 2 mm (from top: first set of panels in **a**); 200 μ m (insets in **a**); 100 μ m (**c**, and from top: second, third, and fourth sets of panels in **a**); 50 μ m (**b**).

of the brain and spinal cord from an animal with this wasting disease, showed the absence of storage material in the entire cerebellum and spinal cord. The brain stem, midbrain, thalamus and hypothalamus showed very little GM2 ganglioside but, commensurate with the neurological signs and behavior, storage-loaded cells were abundant in the cerebral cortex, hippocampus, and olfactory bulbs.

To investigate why some Cx2-injected animals appeared to escape disease and the putative association with specific patterns of glycoconjugate storage, brain and spinal tissue from one such mouse was also stained with the PAS reagent (**Supplementary Video S7**). While PAS-positive neurons in the right brain were scarce (few were present in the striatum, thalamus and cerebral cortex) more extensive involvement was observed in the same

structures of the left brain (**Figure 4c** and **Supplementary Figure S2**). In the spinal cord PAS-positive neurons were rare.

Long-term rescue of CNS permits expression of other disease manifestations

Accumulation of undegraded glycoconjugates has been reported in kidney and liver of patients with SD and in experimental Sandhoff mice; we thus predicted that long-term surviving SD mice would show increased storage in these viscera. Large amounts of storage material were indeed present in these organs, but in addition we found pathology in cell types previously not considered to be affected. At its humane end point, the SD mouse retina shows positive PAS staining only in the ganglion cell layer, but in animals after gene therapy to rescue the central nervous system

(CNS) disease, staining extended also to the inner nuclear layer (Figure 6b). Similarly, in untreated SD mice, the endothelium of the brain and spinal cord appeared free of storage material or other abnormalities. Endothelium of SD mice more than 6 months of age and after gene therapy, stained strongly with the PAS reagent; this was associated with low β -hexosaminidase activity staining of these areas, even though local enzyme activity was clearly sufficient to maintain neighboring neurons and glial cells free of stored glycoconjugate. Endothelial cells appeared free of glycoconjugate where abundant β -hexosaminidase activity was present, such as at loci close to the site of injection (Figure 6c). This would suggest that CNS endothelium is not refractory to enzyme uptake and storage correction, but rather a larger pool of β -hexosaminidase is necessary than for neighboring neurons and glia, possibly due to the blood–brain barrier. The endothelium of peripheral tissues in these animals also stained strongly with the PAS reagent.

Of the animals surviving >1 year with little or no overt neurological signs in groups S+C and H+C, more than one half developed an acute illness which was usually fatal within a few days. Postmortem examination revealed gross urinary and/or fecal retention with massive dilatation of the urinary bladder and/or colon (see **Supplementary Table S1** for details). There was a slight predominance of male mice, compared with females, in relation to the urinary retention, but animals of both genders experienced fecal retention involving the small and large intestine, which we attribute to autonomic neuropathy. Detailed pathological examination by certified veterinarians failed to identify bacterial infections or any other cause of death. In this context however, it is notable that some animals remained healthy for at least 2 years.

DISCUSSION

The GM2 gangliosidoses are emblematic lysosomal diseases which cause fatal neurodegeneration in young infants. Mice with SD show a latent phase during the first few months of life only to enter a phase of rapid decline which is lethal within 6 weeks.^{15,16,29} This animal model thus constitutes an invaluable framework by which to explore and stringently test prospective therapies, such as gene transfer.

We and others have shown that intracranial application of gene-,^{23,27} cell-,^{19,20} and protein-²² based therapies can alleviate, albeit with marked differences in efficacy, the progressive accumulation of storage material and clinical signs in the GM2 gangliosidosis mouse models. Results from these studies have shown that resolution of pathology extends to regions beyond the primary source of enzyme. This is facilitated by secretion of β -hexosaminidase by competent cells into interstitial spaces that can then be recaptured by cells at a distance³⁰—a property shared with other lysosomal hydrolases.

We show here for the first time rescue of GM2 gangliosidosis in brain and spinal cord for up to 2 years in the acute Sandhoff mouse model by rAAV-mediated gene transfer. All three β -hexosaminidase isozymes were generated after coinjection of rAAV α and rAAV β on a single occasion intracranially in young adult mice, and it is possible that some Hex A and Hex S could be chimeric due to coassembly with the endogenous mouse α subunit.

Our results show the value of exploiting the intricate interconnectivity of the brain to promote viral and enzyme distribution

for diseases that affect the nervous system diffusely, as were those reported by others.^{31,32} However, by targeting gene therapy to specific structures, we were able to discriminate the tremor and ataxic signs from the spastic manifestations. Critically, very small differences in the amount and/or distribution of recombinant protein determine whether this intervention succeeds or fails. These findings suggest the existence of threshold effects *in vivo*—that restoration of a small percentage of wild-type activity would be sufficient to restore GM2 degradation to normal—and that small variations below this target would adversely affect the course of disease.³³

We observed a remarkable dissemination of therapeutic protein distributed through the perivascular space in the brain and spinal cord of Sandhoff mice. This route of enzyme movement appears to contribute importantly to maintaining neural tissue free of storage and inflammation. In support of our findings are studies by Lie and colleagues, who, after injecting rAAV4 into the lateral ventricle of MPS VII mice, showed recombinant β -glucuronidase in close association with brain microvasculature—which they attributed to CSF flow.³⁴ Broekman *et al.* also identified β -galactosidase in the perivascular space of Virchow–Robin after hippocampal infusions of rAAV 2/1 in GM1 gangliosidosis mice.³⁵ Cserr and colleagues, and others, confirmed that radioactive tracers of different molecular weights injected into the brain parenchyma were distributed along perivascular spaces and cleared at similar rates—consistent with convective bulk flow, rather than diffusion.^{36,37} Recently, the purified lysosomal enzyme acid sphingomyelinase was injected into the lateral ventricles of the Rhesus macaque and was detected in perivascular spaces.³⁸ Here, we report that 2 years after rAAV infusions, choroid plexus, and brain parenchyma still expressed vector RNA and protein—and thus, β -hexosaminidase would be expected to be secreted into the CSF and interstitial parenchyma. Although we have not demonstrated “flow” of enzyme or the direction of the putative flow, the experimental evidence for its existence is very strong. Weller and colleagues have elegantly characterized perivascular flow in animal models of Alzheimer’s disease, including mice transgenic for the human β -amyloid peptide.^{39,40} These findings, and those of others,^{36–38} will guide the design of further experiments to define more precisely the perivascular route of enzyme transport and investigate its significance for the therapeutic outcomes in GM2 gangliosidosis that we find.

That the small viral dose injected was sufficient to transduce brain parenchyma extensively and that vector was also distributed widely via the CSF space, was unexpected. With few cells reacting positively for vector RNA by ISH and the absence of detectable glycoconjugates in neurons throughout the entire length of the spinal cord, secretion of β -hexosaminidase by choroid plexus is likely to have contributed substantially to the spread of enzyme. We cannot exclude the presence of some vector RNA in cells that was not detected by the ISH stain. Vector RNA and enzyme in dorsal root ganglia cell bodies correlate with prominent labeling of gray matter and roots in dorsal horn and corresponding spinal nerves. Similar distribution of horseradish peroxidase after infusion into the lateral ventricles or subarachnoid space of cats has been reported.^{41,42}

The accepted view that substances in the CSF inevitably drain from subarachnoid space through arachnoid granulations and out

into cerebral veins is not consistent with our findings. In agreement with other studies, our findings indicate that much of the CSF containing rAAV and/or protein travels along the meningeal sheaths such as those of cranial nerves, and drains into extracerebral tissue.⁴³ Having arrived at these sites, the virus is then able to enter permissive cells such as muscle. The brain is an immuno-privileged site but dissemination from the CNS to lymph tissue would allow direct access of potentially antigenic material with the possibility of inducing an immune response,⁴⁰ rendering immunosuppression an important consideration during the planning of clinical trials.

The strong lateralization of storage clearance in rostral brain structures after we injected rAAV into the hindbrain, suggests that in addition to the well-recognized motor fibers that decussate in the midbrain, ipsilateral fibers exist that can transport enzyme to these distant regions. We identified the transduced locus coeruleus as a potential source of this effect. This locus has ipsilateral projections with widespread distribution throughout the neuraxis⁴⁴—and would be an excellent target for many gene therapy applications for diffuse CNS diseases.

We contend that the unprecedented survival and correction of the pathology achieved in the CNS in this acute animal model of GM2 gangliosidosis results from the exploitation of several routes of vector and protein distribution: axonal-, CSF-, and perivascular transport, as well as diffusion. Given that each neuron has its own capillary for oxygen and nutrient supply, we believe that the perivascular route merits further investigation.

We attribute the catastrophic visceral disease that occurred in some of the long-surviving mice to autonomic neuropathy. It is noteworthy that autonomic abnormalities have been reported in rare adults with human SD.⁴⁵

It has been estimated that to use AAV-mediated gene therapy for distributing lysosomal enzymes globally to the brain of an infant would require >50 individual intraparenchymal injections³¹ and clearly for optimal clinical utility, improved means of delivery are required. To treat the human brain and spinal cord, we propose that a combination of convection-enhanced delivery to the parenchyma,⁴⁶ with intraventricular and/or intrathecal injections of rAAV vectors is more realistic. Here we have shown that coinjection of monocistronic vectors, each expressing one or other of the human subunits is an effective means to secure appropriate HexA biosynthesis *in vivo* and offers a practical approach for treating the GM2 gangliosidosis. In relation to the Sandhoff, rather than the Tay–Sachs variant of GM2 gangliosidosis, the hitherto unknown emergence of peripheral disease in long-term survivors after the neurological features are corrected, should be taken into account—so that ultimately a combinatorial stratagem to treat systemic and CNS disease may be needed.

MATERIALS AND METHODS

Experimental animals. The knockout SD mouse model (strain: B6; 129S-Hexbtm1Rlp) was obtained from the Jackson Laboratory (Bar Harbor, ME).¹⁵ The strain was maintained by crossing homozygous males with heterozygous females or by heterozygous matings. These studies were conducted by using protocols approved under license by the U.K. Home Office (Animals Scientific Procedures Act, 1986). *hexb* genotyping was determined by PCR as previously described.²⁷ Mice were provided with nutritional supplements (Transgel; Charles River Laboratories, Margate, UK) on the cage surface.

The approved humane end point applied to mice throughout these studies, was defined as the loss of between 10 and 20% of presymptomatic body weight. Animals were killed at any time if they developed clinical signs such as visceral enlargement, tumors, and self-inflicted injuries or when they reached the age of 2 years.

Vector construction and production. Human cDNAs coding for the α and β subunits were fused at their 3'-ends to human immunodeficiency virus protein transduction domain, woodchuck hepatitis virus posttranscriptional regulatory element (WPPE), and bovine growth hormone polyadenylation signal (BGHpA), as described.²⁷ Recombinant AAV viruses were produced by triple plasmid cotransfection of HEK 293 cells as described.²⁷ Titters were 9×10^{12} and 1.3×10^{13} drps/ml for rAAV2/1 α and rAAV2/1 β , respectively.

Intracranial stereotaxic infusion of rAAV vectors. Four to five-week-old Sandhoff mice were anesthetized and placed in a stereotaxic frame (Kopf Instruments, Tujunga, CA). Burr holes were drilled over target sites, and vector mix was delivered vertically by using coordinates relative to bregma and dura. Single-site injections into the striatum were at: anterior posterior (AP), -0.1 mm; medial-lateral (ML), -2.0 mm; and dorsal-ventral (DV) -3.0 mm. For bilateral injections, into the striatum, AP, -0.1 mm; ML, ± 2.0 mm; and DV, -3.0 mm; the hippocampus, AP, -2.0 ; ML, ± 1.5 ; DV, -2.5 ; and cerebellum, AP, -6.0 mm; ML, ± 1.5 mm; DV, -3.0 mm. Animals received $3 \mu\text{l}$ of vector per site, volume ratio of 1.1: 1.1: 0.8 (rAAV2/1 α : rAAV2/1 β : 20% wt/vol mannitol), at $0.8 \mu\text{l}/\text{minute}$ infusion rate. The needle was withdrawn after 5 minutes. Animals were given postoperative analgesia (Rimadyl, Large Animal Solution; Pfizer, Kent, UK), and placed in an incubator at 37°C to recover.

Tissue processing. Mice were killed and organs either snap-frozen on dry-ice or transcardially perfused with cold phosphate-buffered saline followed by 4% paraformaldehyde. Perfused tissue was post-fixed in the same fixative for a few hours and cryoprotected in 30% sucrose overnight at 4°C . 15 or $45 \mu\text{m}$ coronal sections were cut and stored at -80°C .

Ion-exchange chromatography and fluorimetric analysis. Unfixed tissue was weighed and homogenized at 8% (wt:vol) in cold and degassed 10 mmol/l sodium phosphate (pH 6.0), containing 100 mmol/l NaCl and 0.1% Triton X-100. Extracts were loaded into a Resource Q column (# 17-1177-01; GE Healthcare, Little Chalfont, UK) and run in the fast performance liquid chromatography system ÄKTA Purifier 10 using the UNICORN 5.1 software package (GE Healthcare). After extensive washing with 2 mol/l NaCl followed by loading buffer, the column was developed with 10 ml of an NaCl gradient from 100 to 400 mmol/l, and 0.5 ml fractions collected and stored on ice until fluorimetrically analyzed. Five microliters of unfractionated lysate extracts and fractions were assayed for β -hexosaminidase activity with 4-methylumbelliferyl-2-acetamido-2-deoxy- β -D-glucopyranoside (MU-GlcNAc, 4-MUG) (Biosynth AG, Kings Langley, UK) in 0.01 mol/l phosphate citrate buffer pH 4.4; and 4-methylumbelliferyl-6-sulfo-2-acetamido-2-deoxy- β -D-glucopyranoside (MU-GlcNAc-6-SO₄, 4-MUGS) (Melford Laboratories, Ipswich, UK) in 0.2 mol/l phosphate citrate buffer pH 4.0. Fluorescence was determined in a Perkin Elmer Precisely 1420 Multilabel Counter Victor 3 (excitation: 355 nm; emission: 460 nm).

Polyacrylamide gel electrophoresis and cellulose-acetate electrophoresis. For polyacrylamide gel electrophoresis, tissue extracts were run in 4–15% linear gradient gels (#161-1122; Bio-Rad, Hemel Hempstead, UK) in the presence of sodium dodecyl sulfate. Western blots were processed with goat polyclonal antihuman HexA antibody (kindly donated by Dr R.L. Proia) which detects both α and β subunits²⁶ and secondary antibody rabbit anti-goat-HRP (1/5,000; DakoCytomation, Ely, UK). Blots were developed with LumiGLO chemiluminescent substrate (KPL).

Tissue extracts, containing between 100 and $250 \mu\text{g}$ of protein were applied to a cellulose-acetate gel (Cellogel; Accurate Chemical & Scientific,

Westbury, UK), run in 20 mmol/l phosphate buffer pH 7.0, and incubated in 20 mmol/l citrate-phosphate buffer pH 4.4, containing 2.5 mmol/l 4-MUG substrate at 37°C for 1 hour. Enzyme activity was visualized as fluorescence under UV light, essentially as described.²⁶ Protein was quantified by the Pierce protein assay (MicroBCA Reagent).

Histological staining. For nonperfused tissue, sections were warmed up at room temperature for ~30 minutes and fixed in cold 4% paraformaldehyde for 10 minutes before staining. β -Hexosaminidase activity was detected with naphthol AS-BI *N*-acetyl- β -glucosaminidase (Sigma, Poole Dorset, UK);⁴⁷ and for dual detection of blood vessels, sections were then incubated with fluorescein-conjugated tomato lectin (1/100; *Lycopersicon esculentum*; Vector Laboratories, Peterborough, UK). PAS (Sigma) stained sections were counterstained with hematoxylin. Before mounting in dibutyl phthalate xylene from BDH, sections were dehydrated and cleared with a series of ethanols and xylene. Lectin-labeled sections were directly mounted in diamidino-2-phenylindole containing ProLong Gold antifade reagent (Invitrogen, Paisley, UK) and images collected with a NIKON TE-300 fluorescence microscope (Nikon, Kingston, UK).

Immunohistological staining was performed with mouse monoclonal anti-*N*-acetyl-GM2 immunoglobulin M (MK1-16; Seikagaku, Tokyo, Japan; 1/100), rat anti-mouse CD68 (MCA1957; Serotec, Oxford, UK; 1/50), goat anti-GFAP (N-18, Santa Cruz Biotechnology, Calne, UK; 1/50) as primary antibodies. Staining was based on the avidin-biotin peroxidase technique (Vectastain ABC HP kit; Vector Laboratories), developed with 3'-diaminobenzidine and counterstained with Cresyl violet. Biotinylated secondary antibodies were goat anti-mouse immunoglobulin M μ -chain (Jackson ImmunoResearch, Newmarket, UK), rabbit anti-rat IgG and rabbit anti goat IgG from Vector Laboratories. Slides were mounted with dibutyl phthalate xylene as described above.

ISH was performed with digoxigenin or fluorescein labeled riboprobes against the WPRE-BGHPA sequence, present in both rAAV α and rAAV β vectors, or against human β -hexosaminidase α (684 bases long; cDNA positioned 782–1,466) or β (852 bases long; cDNA positioned 314–1,166) subunit sequences.⁴⁸ ISH-positive cells were detected by colorimetric staining with alkaline phosphatase-mediated BCIP (5-bromo-4-chloro-3-indolylphosphate)-nitroblue tetrazolium reaction, essentially as described⁴⁹ or tyramide signal amplification reagent (TSA) following manufacturer's recommendations. Fluorescein-TSA and cyanine 3-TSA were from Perkin Elmer, Waltham, MA (TSA kits) and anti-digoxigenin-POD and anti-fluorescein-POD were from Roche (Burgess Hill, UK). Sections were directly mounted in diamidino-2-phenylindole containing ProLong Gold antifade reagent and images collected with NIKON TE-300 fluorescence microscope and confocal Leica TCS SPE (Leica Microsystems, Milton Keynes, UK).

Statistics. The Kaplan–Meier survival curve was analyzed with the log-rank equivalent to the Mantel–Cox test. The statistics were analyzed with one-way analysis of variance and Bonferroni multiple *post-hoc* comparisons. Statistical analyses were performed with GraphPad Prism v5.0 (GraphPad Software). Values with $P < 0.05$ were considered significant.

The mean value of weekly weights, across all mice in each group, is calculated for each week of age along with the associated SE, and the mean \pm 1.96 SE are plotted against the mid-point of each week. Assuming individual observations within each week to be independent and normally distributed, the vertical bars represent 95% confidence intervals for the estimated means.

SUPPLEMENTARY MATERIAL

Figure S1. Comparison of average weekly weights between controls and rAAV α +rAAV β -injected mice.

Figure S2. Pattern of vector RNA expression and glycoconjugate storage in a Cx2-injected Sandhoff mouse.

Figure S3. Glycoconjugate storage and neuroinflammation is decreased at sites with prominent perivascular β -hexosaminidase.

Figure S4. Glycoconjugate storage compared between WT, untreated and S+C-treated Sandhoff mice.

Table S1. Cause of death of the animals in this study.

Table S2. Structures stained for vector RNA by *in situ* hybridization (ISH) after Cx2, Sx2, and H+C injections into Sandhoff mice.

Video 1. Untreated SD mouse at the humane end point of 120 days of age.

Video 2. S+C-treated SD mouse at 1 year of age. Classical features of disease are absent.

Video 3. The same S+C-treated mouse as in **Supplementary Video S2** seen here at 2 years of age accompanied by untreated normal littermate.

Video 4. Sx2-treated SD mouse at 1 year of age.

Video 5. The same Sx2-treated mouse as in video 4 at 20 months of age.

Video 6. Cx2-treated SD mouse at the humane end point of 265 days of age.

Video 7. Cx2-treated SD mouse at 1 year of age.

ACKNOWLEDGMENTS

We gratefully acknowledge support from The National Institute of Health Research-Biomedical Research Centre, an unrestricted grant from Cambridge in America, CLIMB (Children Living with Inherited Metabolic Disorders) National Tay–Sachs and Allied Diseases Association, MRC Link Programme Award, The Paul Morgan Trust and MRC core-funding (grant code U.1052.00.005). We thank Dr Passini for generously providing protocol and advice on ISH staining and Dr Proia for providing anti-Hex A antibody.

REFERENCES

- Johnson, WG (1981). The clinical spectrum of hexosaminidase deficiency diseases. *Neurology* **31**: 1453–1456.
- Kolodny, EH, Brady, RO and Volk, BW (1969). Demonstration of an alteration of ganglioside metabolism in Tay–Sachs disease. *Biochem Biophys Res Commun* **37**: 526–531.
- Okada, S and O'Brien, JS (1969). Tay–Sachs disease: generalized absence of a beta-D-*N*-acetylhexosaminidase component. *Science* **165**: 698–700.
- Sandhoff, K (1969). Variation of beta-*N*-acetylhexosaminidase-pattern in Tay–Sachs disease. *FEBS Lett* **4**: 351–354.
- Conzelmann, E and Sandhoff, K (1979). Purification and characterization of an activator protein for the degradation of glycolipids GM2 and GA2 by hexosaminidase A. *Hoppe-Seyler's Z Physiol Chem* **360**: 1837–1849.
- Robinson, D and Carroll, M (1972). Tay–Sachs disease: interrelation of hexosaminidases A and B. *Lancet* **1**: 322–323.
- Conzelmann, E and Sandhoff, K (1978). AB variant of infantile GM2 gangliosidosis: deficiency of a factor necessary for stimulation of hexosaminidase A-catalyzed degradation of ganglioside GM2 and glycolipid GA2. *Proc Natl Acad Sci USA* **75**: 3979–3983.
- Srivastava, SK, Wiktorowicz, JE and Awasthi, YC (1976). Interrelationship of hexosaminidases A and B: conformation of the common and the unique subunit theory. *Proc Natl Acad Sci USA* **73**: 2833–2837.
- Conzelmann, E and Sandhoff, K (1978). AB variant of infantile GM2 gangliosidosis: deficiency of a factor necessary for stimulation of hexosaminidase A-catalyzed degradation of ganglioside GM2 and glycolipid GA2. *Proc Natl Acad Sci USA* **75**: 3979–3983.
- Myerowitz, R, Lawson, D, Mizukami, H, Mi, Y, Tiffit, CJ and Proia, RL (2002). Molecular pathophysiology in Tay–Sachs and Sandhoff diseases as revealed by gene expression profiling. *Hum Mol Genet* **11**: 1343–1350.
- Wada, R, Tiffit, CJ and Proia, RL (2000). Microglial activation precedes acute neurodegeneration in Sandhoff disease and is suppressed by bone marrow transplantation. *Proc Natl Acad Sci USA* **97**: 10954–10959.
- Wu, YP and Proia, RL (2004). Deletion of macrophage-inflammatory protein 1 alpha retards neurodegeneration in Sandhoff disease mice. *Proc Natl Acad Sci USA* **101**: 8425–8430.
- Cork, LC, Munnell, JF, Lorenz, MD, Murphy, JV, Baker, HJ and Rattazzi, MC (1977). GM2 ganglioside lysosomal storage disease in cats with beta-hexosaminidase deficiency. *Science* **196**: 1014–1017.
- Porter, BF, Lewis, BC, Edwards, JF, Alroy, J, Zeng, BJ, Torres, PA *et al.* (2011). Pathology of GM2 gangliosidosis in Jacob sheep. *Vet Pathol* **48**: 807–813.
- Sango, K, Yamanaka, S, Hoffmann, A, Okuda, Y, Grinberg, A, Westphal, H *et al.* (1995). Mouse models of Tay–Sachs and Sandhoff diseases differ in neurologic phenotype and ganglioside metabolism. *Nat Genet* **11**: 170–176.
- Phaneuf, D, Wakamatsu, N, Huang, JQ, Borowski, A, Peterson, AC, Fortunato, SR *et al.* (1996). Dramatically different phenotypes in mouse models of human Tay–Sachs and Sandhoff diseases. *Hum Mol Genet* **5**: 1–14.
- Andersson, U, Smith, D, Jeyakumar, M, Butters, TD, Borja, MC, Dwek, RA *et al.* (2004). Improved outcome of *N*-butyldeoxygalactonojirimycin-mediated substrate reduction therapy in a mouse model of Sandhoff disease. *Neurobiol Dis* **16**: 506–515.
- Jeyakumar, M, Norflus, F, Tiffit, CJ, Cortina-Borja, M, Butters, TD, Proia, RL *et al.* (2001). Enhanced survival in Sandhoff disease mice receiving a combination of substrate deprivation therapy and bone marrow transplantation. *Blood* **97**: 327–329.

19. Lee, JP, Jeyakumar, M, Gonzalez, R, Takahashi, H, Lee, PJ, Baek, RC *et al.* (2007). Stem cells act through multiple mechanisms to benefit mice with neurodegenerative metabolic disease. *Nat Med* **13**: 439–447.
20. Lacorazza, HD, Flax, JD, Snyder, EY and Jendoubi, M (1996). Expression of human beta-hexosaminidase alpha-subunit gene (the gene defect of Tay-Sachs disease) in mouse brains upon engraftment of transduced progenitor cells. *Nat Med* **2**: 424–429.
21. Jeyakumar, M, Smith, DA, Williams, IM, Borja, MC, Neville, DC, Butters, TD *et al.* (2004). NSAIDs increase survival in the Sandhoff disease mouse: synergy with N-butyldeoxynojirimycin. *Ann Neurol* **56**: 642–649.
22. Matsuoka, K, Tamura, T, Tsuji, D, Dohzono, Y, Kitakaze, K, Ohno, K *et al.* (2011). Therapeutic potential of intracerebroventricular replacement of modified human β -hexosaminidase B for GM2 gangliosidosis. *Mol Ther* **19**: 1017–1024.
23. Guidotti, JE, Mignon, A, Haase, G, Caillaud, C, McDonnell, N, Kahn, A *et al.* (1999). Adenoviral gene therapy of the Tay-Sachs disease in hexosaminidase A-deficient knock-out mice. *Hum Mol Genet* **8**: 831–838.
24. Kyrkanides, S, Miller, JN, Tallents, RH, Broukhon, SM, Centola, GM and Olschowka, JA (2007). Intraperitoneal inoculation of Sandhoff mouse neonates with an HIV-1 based lentiviral vector exacerbates the attendant neuroinflammation and disease phenotype. *J Neuroimmunol* **188**: 39–47.
25. Tropak, MB, Reid, SP, Guiral, M, Withers, SG and Mahuran, D (2004). Pharmacological enhancement of beta-hexosaminidase activity in fibroblasts from adult Tay-Sachs and Sandhoff Patients. *J Biol Chem* **279**: 13478–13487.
26. Proia, RL, d’Azzo, A and Neufeld, EF (1984). Association of alpha- and beta-subunits during the biosynthesis of beta-hexosaminidase in cultured human fibroblasts. *J Biol Chem* **259**: 3350–3354.
27. Cachón-González, MB, Wang, SZ, Lynch, A, Ziegler, R, Cheng, SH and Cox, TM (2006). Effective gene therapy in an authentic model of Tay-Sachs-related diseases. *Proc Natl Acad Sci USA* **103**: 10373–10378.
28. Franklin, KBJ and Paxinos, G (2001). *The Mouse Brain in Stereotaxic Coordinates*. 2nd edn. Academic Press: San Diego, CA.
29. Miklyayeva, EI, Dong, W, Bureau, A, Fattahie, R, Xu, Y, Su, M *et al.* (2004). Late onset Tay-Sachs disease in mice with targeted disruption of the Hexa gene: behavioral changes and pathology of the central nervous system. *Brain Res* **1001**: 37–50.
30. Thomas, GH, Taylor, HA, Miller, CS, Axelman, J and Migeon, BR (1974). Genetic complementation after fusion of Tay-Sachs and Sandhoff cells. *Nature* **250**: 580–582.
31. Passini, MA, Lee, EB, Heuer, GG and Wolfe, JH (2002). Distribution of a lysosomal enzyme in the adult brain by axonal transport and by cells of the rostral migratory stream. *J Neurosci* **22**: 6437–6446.
32. Martino, S, Marconi, P, Tancini, B, Dolcetta, D, De Angelis, MG, Montanucci, P *et al.* (2005). A direct gene transfer strategy via brain internal capsule reverses the biochemical defect in Tay-Sachs disease. *Hum Mol Genet* **14**: 2113–2123.
33. Conzelmann, E and Sandhoff, K (1983). Partial enzyme deficiencies: residual activities and the development of neurological disorders. *Dev Neurosci* **6**: 58–71.
34. Liu, G, Martins, J, Wemmie, JA, Chiorini, JA and Davidson, BL (2005). Functional correction of CNS phenotypes in a lysosomal storage disease model using adeno-associated virus type 4 vectors. *J Neurosci* **25**: 9321–9327.
35. Broekman, ML, Tierney, LA, Benn, C, Chawla, P, Cha, JH and Sena-Esteves, M (2009). Mechanisms of distribution of mouse beta-galactosidase in the adult GM1-gangliosidosis brain. *Gene Ther* **16**: 303–308.
36. Cserr, HF and Patlak, CS (1992). Secretion and bulk flow of interstitial fluid. In: Bradbury, M.W.B. (ed.). *Physiology and Pharmacology of the Blood-Brain Barrier*. Springer: Berlin, 245–261.
37. Hadaczek, P, Yamashita, Y, Mirek, H, Tamas, L, Bohn, MC, Noble, C *et al.* (2006). The “perivascular pump” driven by arterial pulsation is a powerful mechanism for the distribution of therapeutic molecules within the brain. *Mol Ther* **14**: 69–78.
38. Ziegler, RJ, Salegio, EA, Dodge, JC, Bringas, J, Treleaven, CM, Bercury, SD *et al.* (2011). Distribution of acid sphingomyelinase in rodent and non-human primate brain after intracerebroventricular infusion. *Exp Neurol* **231**: 261–271.
39. Weller, RO, Djuanda, E, Yow, HY and Carare, RO (2009). Lymphatic drainage of the brain and the pathophysiology of neurological disease. *Acta Neuropathol* **117**: 1–14.
40. Carare, RO, Bernardes-Silva, M, Newman, TA, Page, AM, Nicoll, JA, Perry, VH *et al.* (2008). Solutes, but not cells, drain from the brain parenchyma along basement membranes of capillaries and arteries: significance for cerebral amyloid angiopathy and neuroimmunology. *Neuropathol Appl Neurobiol* **34**: 131–144.
41. Brierley, JB (1950). The penetration of particulate matter from the cerebrospinal fluid into the spinal ganglia, peripheral nerves, and perivascular spaces of the central nervous system. *J Neurol Neurosurg Psychiatr* **13**: 203–215.
42. Rennels, ML, Gregory, TF, Blaumanis, OR, Fujimoto, K and Grady, PA (1985). Evidence for a ‘paravascular’ fluid circulation in the mammalian central nervous system, provided by the rapid distribution of tracer protein throughout the brain from the subarachnoid space. *Brain Res* **326**: 47–63.
43. Arnold, W, Nitze, HR and Ritter, R (1971). Anatomical relations between the cerebrospinal fluid (CSF) and the lymphatic system in the region of the head and neck. *Arch Klin Exp Ohren Nasen Kehlkopfteilkd* **198**: 361.
44. Jones, BE and Moore, RY (1977). Ascending projections of the locus coeruleus in the rat. II. Autoradiographic study. *Brain Res* **127**: 25–53.
45. Pellegrini, M, Zicari, E, Dotti, MT and Federico, A (2006). Dysautonomic achalasia in two siblings with Sandhoff disease. *J Neurol Sci* **241**: 107–109.
46. Salegio, EA, Kells, AP, Richardson, RM, Hadaczek, P, Forsyeth, J, Bringas, J *et al.* (2010). Magnetic resonance imaging-guided delivery of adeno-associated virus type 2 to the primate brain for the treatment of lysosomal storage disorders. *Hum Gene Ther* **21**: 1093–1103.
47. Lacorazza, HD and Jendoubi, M (1995). In situ assessment of beta-hexosaminidase activity. *BioTechniques* **19**: 434–440.
48. Bapat, B, Ethier, M, Neote, K, Mahuran, D and Gravel, RA (1988). Cloning and sequence analysis of a cDNA encoding the beta-subunit of mouse beta-hexosaminidase. *FEBS Lett* **237**: 191–195.
49. Barthel, LK and Raymond, PA (2000). In situ hybridization studies of retinal neurons. *Meth Enzymol* **316**: 579–590.